International Journal of Nanomedicine

Dovepress
open access to scientific and medical research

Open Access Full Text Article

ORIGINAL RESEARCH

Folate-receptor-targeted laser-activable poly(lactide-*co*-glycolic acid) nanoparticles loaded with paclitaxel/indocyanine green for photoacoustic/ultrasound imaging and chemo/photothermal therapy

This article was published in the following Dove Press journal:
International Journal of Nanomedicine

Fengqiu Liu[1,2]
Yuli Chen[1,2]
Yizhen Li[1,2]
Yuan Guo[1,2]
Yang Cao[1,2]
Pan Li[1,2]
Zhigang Wang[1,2]
Yuping Gong[1,2,*]
Haitao Ran[1,2,*]

[1]Ultrasound Department, Second Affiliated Hospital, Chongqing Medical University, [2]Chongqing Key Laboratory of Ultrasound Molecular Imaging, Chongqing, China

*These authors contributed equally to this work

Correspondence: Haitao Ran; Yuping Gong
Second Affiliated Hospital of Chongqing Medical University, 76 Linjiang Road, Chongqing, 400010, China
Tel +86 23 6369 3180; +86 23 6369 3172
Email rht66@163.com; gongyuping1982@163.com

Background: Cancer is one of the most serious threats to human health. Precision medicine is an innovative approach to treatment, as part of which theranostic nanomedicine has been studied extensively. However, the required biocompatibility and substantial cost for the approval of nanomedicines hinder their clinical translation.

Purpose: We designed a novel type of theranostic nanoparticle (NP) folate-receptor-targeted laser-activatable poly(lactide-*co*-glycolic acid) (PLGA) NPs loaded with paclitaxel (Ptx)/indocyanine green (ICG)-folic acid-polyethylene glycol (PEG)-PLGA-Ptx@ICG-perfluorohexane (Pfh)- using safe and approved materials and drugs, which would facilitate clinical translation. With laser irradiation, highly efficient photothermal therapy can be achieved. Additionally, targeted NPs can be activated by near-infrared laser irradiation at a specific region, which leads to the sharp release of Ptx at areas of high folate-receptor expression and ensures a higher Ptx concentration within the tumor region, thereby leading to chemo/photothermal synergistic antitumor efficacy. Meanwhile, the NPs can be used as a dual-modality contrast agent for photoacoustic and ultrasound imaging.

Materials and methods: FA-PEG-PLGA-Ptx@ICG-Pfh NPs were prepared by sonification method and characterized for physicochemical properties. Cytotoxicity and in vivo biocompatibility were evaluated respectively by CCK8 assay and blood analysis. NPs as dual-modality contrast agents were evaluated by photoacoustic/ultrasound imaging system in vitro and in vivo. In vitro anticancer effect and in vivo anticancer therapy was evaluated by CCK8 assay and MDA-MB231 tumor-bearing mice model.

Results: FA-PEG-PLGA-Ptx@ICG-Pfh NPs were in the size of 308±5.82 nm with negative zeta potential and showed excellent photothermal effect. The NPs could be triggered sharp release of Ptx by laser irradiation, and showed the good biocompatibility in vitro and in vivo. Through photoacoustic/ultrasound imaging, the NPs showed an excellent ability as dual-modality contrast agents in vitro and in vivo. FA-PEG-PLGA-Ptx@ICG-Pfh NPs with laser irradiation showed the best anticancer efficacy in vitro and in vivo.

Conclusion: Such a biocompatible and novel theranostic NP is expected to integrate dual-modality imaging with improved therapeutic efficacy and provide a promising paradigm for cancer therapy.

Keywords: nanomedicine, folate-receptor-targeted nanoparticle, theranostics, targeted drug-delivery system, combined anticancer therapy, photoacoustic imaging, ultrasound imaging

submit your manuscript | www.dovepress.com
Dovepress
http://dx.doi.org/10.2147/IJN.S167043

Introduction

Cancer is one of the most urgent health concerns and a difficult disease to treat. For significant therapeutic efficacy, improved diagnostic and therapeutic techniques with high precision and minimal side effects are required urgently.[1] The Precision Medicine Initiative is an innovative approach to health care, in which cancer treatment is a major concern.[2,3] However, clinical translation is difficult, in that many experiments and preclinical trials are needed for approval, which requires tremendous costs. Meanwhile, drug discovery has slowed, and only a small proportion of proposed medications are successfully translated into prescriptive and approved therapeutics.[4,5] Therefore, we constructed a novel theranostic nanoparticle (NP) using safe and approved materials and drugs with minimally invasive and alternative chemo/photothermal therapy to facilitate clinical translation. Herein, folic acid (FA)–polyethylene glycol (PEG)–poly(lactide-*co*-glycolic acid) (PLGA)–paclitaxel (Ptx)/indocyanine green (ICG)–perfluorohexane (Pfh) NPs were developed.

In recent years, PLGA has been studied as a biocompatible polymer for the preparation of NPs.[6,7] For its excellent biocompatibility and biodegradability, PLGA was approved by the US Food and Drug Administration (FDA), and has been widely used in pharmaceuticals for many years.[8,9] To avoid serum protein binding and achieve an enhanced permeability and retention (EPR) effect, PEG-functionalized PLGA was introduced in this study. Another compound approved by the FDA, PEG is used widely as a biocompatible polymer that can reduce the accumulation in the mononuclear phagocyte system and prolong the blood half-life of various NPs and nanocomplexes.[10,11]

ICG is an organic dye approved by the FDA for human medical imaging and diagnosis in clinical applications.[12] It is a water-soluble tricarbocyanine dye that absorbs strongly in the near-infrared (NIR) region at approximately 800 nm, which leads to an effective photothermal conversion rate.[13] ICG has been used widely in photothermal therapy (PTT) with a highly efficient photothermal conversion rate, and has been applied as a contrast agent for photoacoustic (PA) imaging.[14]

Folate is a B vitamin and micronutrient for humans,[15] and it can bind to the folate receptor through ligand–receptor interactions.[16] The folate receptor has been studied widely as a molecular target for cancer therapy in recent years, and is overexpressed on the cytomembrane of various solid-tumor cells, including those of breast, lung, prostate, ovarian, brain, and colorectal cancer. Folate-functionalized NPs can target folate-receptor-overexpressing cells.[17]

Owing to its low boiling point (56°C at 1 atm) and phase-change ability (from liquid to gas), Pfh has been used widely in NP construction in recent years.[18–20] NP-encapsulated liquid Pfh can transform into microbubbles when trigged by acoustic droplet vaporization and optical droplet vaporization, thus increasing their echogenicity in ultrasound (US) imaging.[21] Meanwhile, these microbubbles generated in situ can trigger local drug release, resulting in reduced side effects.[22] PTT has been widely studied in cancer treatment, and employs photoabsorbers and NIR lasers to provide precise and minimally invasive alternative cancer therapy.[23] In particular, PTT combined with chemotherapy can achieve a synergistic anticancer effect and significantly reduce tumor recurrence.[24,25]

In this study, we used these safe and approved materials and drugs to construct folate-receptor-targeted multifunctional NPs, ie, FA-PEG-PLGA-Ptx@ICG-Pfh NPs, and applied them not only as a contrast agent for diagnostic imaging but also for anticancer therapy. It was hypothesized that the folate on the surface of the NPs would contribute to the selective binding of the NPs to folate-receptor-positive cancer cells, leading to enhanced intracellular uptake and anticancer efficacy via a laser-triggered drug-delivery system combined with PTT. Meanwhile, owing to the excellent PA imaging characteristic of ICG and the phase-change ability of Pfh, these novel NPs could serve as a dual-modality contrast agent for PA and US imaging.

Methods

Materials and reagents

ICG, polyvinyl alcohol, folate, Ptx, DiI (1,1′-dioctadecyl-3,3,3′,3′-tetramethylindocarbocyanine perchlorate), DAPI (4′,6-diamidino-2-phenylindole) were purchased from Sigma-Aldrich (St Louis, MO, USA). Methoxy-PEG-PLGA (molecular weight [MW] 12,000 Da), carboxyl-PLGA (COOH–PLGA) (MW 12,000 Da), and amino-PEG-amino (NH_2-PEG-NH_2) were purchased from Daigang Biomaterial (Jinan, China). Molecular biology-grade agarose and DiR (1,1′-dioctadecyl-3,3,3′,3′-tetramethylindotricarbocyanine iodide) were purchased from Thermo Fisher Scientific (Waltham, MA, USA). Pfh was purchased from Apollo Scientific (Stockport, UK). MDA-MB231 human breast cancer cells, A549 human lung adenocarcinoma cells, and human umbilical vein endothelial cells (HUVECs) were purchased from the China Center for Type Culture Collection (Wuhan, China). Deionized water obtained from the Millipore system (Direct-Q 5, FRA) was used in all preparations.

Preparation of FA-PEG-PLGA-Ptx@ICG-Pfh NPs

First, 2 mg ICG was dissolved in 200 μL water and mixed with 200 μL Pfh. Then, the mixture was emulsified using

a sonicator (VCX130; Sonics and Materials, Newton, CT, USA) at 100 W for 6 minutes (5 seconds on, 5 seconds off), from which the primary emulsion was obtained. Second, 50 mg FA-PEG-PLGA and 5 mg Ptx were dissolved in 2 mL of dichloromethane, from which the organic solution was obtained. Then, the primary emulsion was added to the organic solution and emulsified using the sonicator at 100 W for 6 minutes (5 seconds on, 5 seconds off). Then, 8 mL 5% polyvinyl alcohol (w:v) was added to the emulsion and further emulsified using a sonicator at 50 W for 4 minutes (5 seconds on, 5 seconds off). To solidify the NP shell, dichloromethane was removed by evaporation. All these procedures were performed in an ice bath. To remove the free ICG and other excess reagents, the emulsion was centrifuged (10,000 rpm, 5 minutes) and washed with water. The centrifugation and washing processes were repeated three times. Finally, the FA-PEG-Ptx@ICG-Pfh NPs were obtained and stored at 4°C. PEG-PLGA-Ptx@ICG-Pfh NPs were prepared the same way, except that FA-PEG-PLGA was replaced with methoxy-PEG-PLGA. To prepare fluorescence-labeled NPs, the fluorescent dye DiI (1 mg) or DiR (1 mg) was added to the organic solution, and other procedures were the same.

Characterization of FA-PEG-PLGA-Ptx@ICG-Pfh NPs

NP size (diameter, nm) and surface charge (ζ-potential, mV) were measured by dynamic light scattering (Zetasizer Nano ZS90, Malvern Instruments, Malvern, UK). First, the FA-PEG-PLGA-Ptx@ICG-Pfh NP solution was diluted to be clear and transparent by ultrapure water. Then, the diluted NP solution was added to sample pools. Last, samples were measured with the Zetasizer.

NP morphology was determined by scanning electron microscopy (SEM; JSM-7800F; JEOL, Tokyo, Japan) at an accelerating voltage of 1 kV and working distance of 10.1 mm. First, a drop of FA-PEG-PLGA-Ptx@ICG-Pfh NP solution was added to the silicon dioxide slice (5×5 mm^2). Then, the silicon dioxide slice was set in a box with desiccants overnight at 4°C. Last, the silicon dioxide slice covered with FA-PEG-PLGA-Ptx@ICG-Pfh NPs was analyzed with SEM.

Assessment of folate on the surface of NPs

Immunofluorescence was applied to assess the binding ability of folate on the surface of the FA-PEG-PLGA-Ptx@ICG-Pfh NPs. To avoid the folate antibody adsorbed on NPs through aspecific binding, firstly NPs were incubated with BSA solution before incubation with the primary antibody. Then, a mouse monoclonal antibody against folate (Hapten and Protein Biomedical Institute, Beijing, China), the primary antibody, was incubated with the NP suspension at a ratio of 1:500 (v:v) for 4 hours at room temperature on the platform of an orbital incubator. Then, NPs were separated by centrifugation (10,000 rpm, 5 minutes) and washed with PBS three times. NPs were then incubated with goat antimouse IgG (fluorescein isothiocyanate) antibody (Abcam, UK), the secondary antibody, at a ratio of 100:1 (v:v) for 1 hour at room temperature on the platform of the orbital incubator. Then, NPs were separated and washed using the same steps as for the primary antibody. Finally, NPs were observed using confocal laser-scanning microscopy (CLSM; A1R-Si; Nikon, Tokyo, Japan).

Temperature elevation and phase change induced by NIR-laser irradiation

To determine whether the FA-PEG-PLGA-Ptx@ICG-Pfh NPs had potential for PTT, the photothermal effect was detected. First, NP solutions of different concentrations were added to 96-well plates and irradiated by an NIR laser for 5 minutes at 1 W/cm^2 (808 nm). Meanwhile, temperature was measured with a thermal imaging camera (Fotric 226; ZXF Laboratories, Allen, TX, USA). To determine whether the FA-PEG-PLGA-Ptx@ICG-Pfh NPs could be transformed into microbubbles by laser irradiation, an observation experiment was carried out. A drop of NP solution (5 mg/mL) was pipetted onto a glass slide and irradiated by an NIR laser for 5 minutes at 1 W/cm^2 (808 nm). Meanwhile, images were captured using inverted microscopy (IX53; Olympus, Tokyo, Japan).

Drug loading and laser-triggered drug release

The encapsulation efficiency (EE) and loading content (LC) of ICG and Ptx were determined using ultraviolet spectrophotometry (Lambda 950; PerkinElmer, Waltham, MA, USA) and high-performance liquid chromatography (HPLC; LC-2010A HT; Shimadzu, Kyoto, Japan), respectively. HPLC analysis was performed on a Welch C_{18} column (ODS; 4.6×250 mm^2, 5 μm). The mobile phase contained a 77:23 mixture of methanol and water with a flow rate of 1 mL/min at 25°C. Signals were detected at a wavelength of 227 nm. EE and LC were calculated thus:

$$EE\,(ICG) = \frac{\text{Total mass of added ICG} - \text{Mass of ICG in supernatant}}{\text{Total mass of added ICG}} \times 100\%$$

$$\text{LC (ICG)} = \frac{\text{Total mass of added ICG} - \text{Mass of ICG in supernatant}}{\text{Mass of NPs}} \times 100\%$$

$$\text{EE (Ptx)} = \frac{\text{Mass of encapsulated Ptx}}{\text{Total mass of added Ptx}} \times 100\%$$

$$\text{LC (Ptx)} = \frac{\text{Mass of encapsulated Ptx}}{\text{Mass of NPs}} \times 100\%$$

To detect the release behavior of FA-PEG-PLGA-Ptx@ICG-Pfh NPs triggered by NIR-laser irradiation, release of Ptx in vitro was assessed. The FA-PEG-PLGA-Ptx@ICG-Pfh NP suspension was equivalently added to different dialysis bags (MW cutoff 10,000 Da). Then, the dialysis bag was placed in a container containing 150 mL buffer solution (30% ethanol, 0.01% Tween 80, 0.02% sodium azide, pH 7.4) under 100 rpm stirring at 37°C. Samples (1 mL each) were collected from the medium at 0.5, 1, 2, 4, 6, 12, and 24 hours and replaced by 1 mL buffer solution. In the laser-irradiation group, the dialysis bag was removed, irradiated with the 808 nm laser (1 W/cm^2) for 5 minutes at 1 hour after sample collection, replaced, and then treated, as were the controls. The samples were analyzed by HPLC and cumulative release ratio calculated.

In vitro gel experiments of PA imaging

The potential of FA-PEG-PLGA-Ptx@ICG-Pfh NPs as contrast agents for PA imaging was assessed using an agar-gel model. A gel phantom 5.0 mm in diameter was constructed using 3% agar (w:v) dissolved in deaerated water. An Eppendorf tube was set in the center of the agar gel to create a void. Next, NP solutions of different concentrations were added to the void for PA imaging using a PA imaging system (Vevo Lazr; Visual Sonics, Toronto, ON, Canada).

In vitro gel experiments of US imaging

The potential of the FA-PEG-PLGA-Ptx@ICG-Pfh NPs as contrast agents for US imaging was assessed using the agar-gel model. The process of making the gel phantom was the same as described for in vitro experiments of PA imaging. NP solutions were added to the void and irradiated with an NIR laser for 5 minutes at 1 W/cm^2 (808 nm). During irradiation, B-mode and contrast-enhanced US (CEUS) images were taken by ultrasonography (MyLab 90; Esaote, Genoa, Italy). Quantitative results were measured with US imaging-analysis software.

Cell culture

MDA-MB231 human breast cancer cells, A549 human lung adenocarcinoma cells, and HUVECs were grown in RPMI 1640 medium (Thermo Fisher Scientific) supplemented with 10% FBS and 1% penicillin–streptomycin in a humidified incubator at 37°C and 5% CO_2.

Animals and tumor model

All animals received care in compliance with the Guidelines for the Care and Use of Laboratory Animals. Female BALB/c nude mice (4–5 weeks old, weighing 18–20 g) were purchased from Beijing HFK Bioscience Corporation and maintained under specific-pathogen-free conditions with free access to food and water. To create the animal model, MDA-MB231 cells (10^6 cells/100 µL) were subcutaneously injected into the left hind limbs of the mice. Tumor-bearing mice were used 2 weeks after the injection (tumor volume up to approximately 0.5 cm^3).

Cytotoxicity assay

To evaluate the cytotoxicity of the FA-PEG-PLGA@ICG-Pfh NPs (Ptx-free) as a multifunctional drug-delivery vehicle, cell viability was measured. MDA-MB231 cells, A549 cells, and HUVECs (5×10^3 cells/well, 100 µL) were seeded into 96-well plates and culture for 12 hours. Then, the original culture media were replaced by NP solutions of different concentrations (diluted with the medium). These cells were cultured continuously for an additional 24 hours. Then, the culture medium was removed and each well was washed three times with PBS. Fresh medium containing Cell Counting Kit 8 (CCK8) reagents (10%) was added, followed by incubation for 2 hours. Absorbance (A_{450}) was measured with a universal microplate reader (ELX800; BioTek Instruments, Winooski, VT, USA). Cell viability was calculated:

$$\frac{A_{450} \text{ of treated cells}}{A_{450} \text{ of control cells}} \times 100\%$$

In vitro cellular uptake

MDA-MB231 cells and A549 cells (5×10^4 cells/well, 1 mL) were seeded onto glass-bottomed cell-culture dishes (Φ 15 mm; Nest Biotechnology, Wuxi, China) and incubated for 12 hours. Then, the original medium was changed to serum-free medium or serum-free medium with added folate and incubated with the cells for another 2 hours. Subsequently, FA-PEG-PLGA@ICG-Pfh or PEG-PLGA@ICG-Pfh NPs labeled with DiI were added to corresponding culture dishes at the same dose (2 mg/mL) and incubated continuously. Incubation was terminated at different time points (0.5, 1, and 2 hours). Then, cells were washed with PBS three times and fixed with 4% formaldehyde solution on ice for 15 minutes.

Cells were then stained with DAPI for 10 minutes, washed with PBS three times, and observed by CLSM.

Anticancer effect

MDA-MB231 cells (5×10^3 cells/well, 100 μL) were seeded into 96-well plates and incubated for 12 hours. Then, different concentrations of NPs (FA-PEG-PLGA-Ptx@ICG-Pfh, PEG-PLGA-Ptx@ICG-Pfh, FA-PEG-PLGA@ICG-Pfh, FA-PEG-PLGA-Ptx@Pfh, or FA-PEG-PLGA@ICG) or free Ptx were added and incubated for 2 hours. Subsequently, each well was washed with PBS three times and 100 μL fresh medium added. Then, after the wells had been irradiated by NIR laser for 5 minutes at 1 W/cm^2 (808 nm), cells were incubated for 24 hours. Finally, cell viability was measured by CCK8 assay.

In vivo biocompatibility

All animal experimental procedures were in agreement with the Guidelines for the Care and Use of Laboratory Animals and approved by the Chongqing Administrative Committee of Laboratory Animals. FA-PEG-PLGA-Ptx@ICG-Pfh NP solutions were administered to 4-week-old female Kunming mice (Laboratory Animal Center of Chongqing Medical University) by intravenous injection at different doses (saline only, 10 mg/kg, 25 mg/kg, 50 mg/kg, n=5 for each group). The mice were killed at day 7 after administration and blood collected to assess liver and renal function and perform routine blood tests.

Biodistribution and tumor accumulation of NPs

The tumor-bearing mice were randomly divided into two groups (n=5 for each group). DiR-labeled FA-PEG-PLGA-Ptx@ICG-Pfh NPs and PEG-PLGA-Ptx@ICG-Pfh NPs were administered by intravenous injection (50 mg/kg, 200 μL). Images were captured using a Xenogen IVIS Spectrum in vivo imaging system (PerkinElmer) at different points before and after administration. After the in vivo imaging process, MDA-MB231 tumor-bearing mice were killed, and the main organs (heart, liver, spleen, lungs, and kidneys) and tumor tissue were analyzed by fluorescence imaging.

In vivo PA imaging

Tumor-bearing mice were randomly divided into two groups (n=5 for each group). FA-PEG-PLGA-Ptx@ICG-Pfh and PEG-PLGA-Ptx@ICG-Pfh NP solutions were administered by intravenous injection (50 mg/kg, 200 μL). Images were captured by the PA imaging system at different points before and after administration.

In vivo US imaging

Tumor-bearing mice were randomly divided into two groups (n=5 for each group). FA-PEG-PLGA-Ptx@ICG-Pfh and PEG-PLGA-Ptx@ICG-Pfh NP solutions were administered by intravenous injection (50 mg/kg, 200 μL). One hour later, the tumor region was irradiated by NIR laser for 5 minutes at 2 W/cm^2 (808 nm). Images were captured by the ultrasonography system before and after irradiation.

In vivo anticancer therapy

Tumor-bearing mice were randomly divided into seven groups (n=8 for each group): FA-PEG-PLGA-Ptx@ICG-Pfh NPs with laser irradiation, PEG-PLGA-Ptx@ICG-Pfh NPs with laser irradiation, FA-PEG-PLGA-Ptx@ICG-Pfh NPs without laser irradiation, FA-PEG-PLGA@ICG-Pfh NPs with laser irradiation, FA-PEG-PLGA-Ptx@Pfh NPs without laser irradiation, Ptx only, FA-PEG-PLGA@ICG NPs without laser irradiation, laser only, and saline. FA-PEG-PLGA-Ptx@ICG-Pfh, PEG-PLGA-Ptx@ICG-Pfh, FA-PEG-PLGA@ICG-Pfh, FA-PEG-PLGA-Ptx@Pfh and FA-PEG-PLGA@ICG NP solutions or Ptx (at the NP-loaded dose) and saline were correspondingly administered by intravenous injection (50 mg/kg, 200 μL). One hour later, the tumor regions of the groups were irradiated by NIR laser for 5 minutes at 2 W/cm^2 (808 nm). Meanwhile, tumor-region temperature was monitored by a thermal imaging camera during irradiation. Tumor size and body weight were measured every 2 days, with tumor volume (V) calculated as $V=L\times W^2/2$, where L is the length and W is the width. Three mice randomly selected from each group were killed at day 3 after irradiation and tumors excised and fixed for immunohistochemical staining. Mice were killed at day 14, and the main organs (heart, liver, spleen, lungs, kidneys) of the mice (FA-PEG-PLGA-Ptx@ICG-Pfh NPs with laser-irradiation group, saline group) were excised and fixed for H&E staining.

Statistical analysis

All data are presented as mean ± SD. Comparisons among groups were analyzed with the use of independent samples by one-way ANOVA using SPSS 18.0, and $P<0.05$ was considered significant.

Results and discussion

Synthesis, preparation, and characterization

The FA-PEG-PLGA polymer was synthesized by Protein Way Biotechnology (Chongqing, China), and to confirm

whether the folate, PEG, and PLGA had successfully bonded, proton nuclear magnetic resonance spectra of the polymer were analyzed. Nuclear magnetic resonance spectra validated the chemical structure of the polymer (Figure S1). FA-PEG-PLGA-Ptx@ICG-Pfh NPs were prepared by US emulsification and purified by centrifugation. NP schematics are given in Figure 1A. NP morphology was determined by SEM. NPs were generally spherical (Figure 1B). NP size was measured

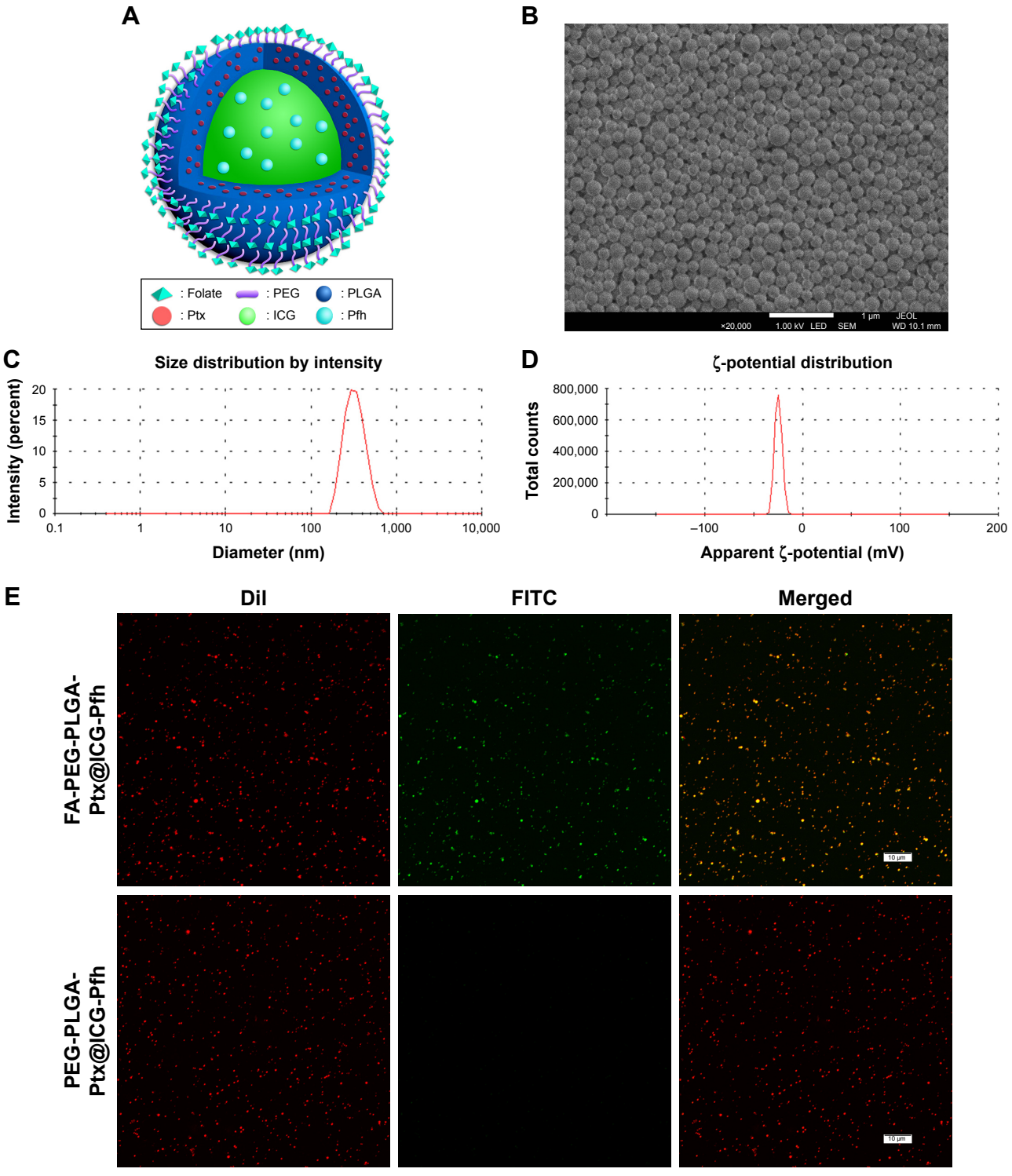

Figure 1 Morphology, structure, and characterization of FA-PEG-PLGA-Ptx@ICG-Pfh NPs.

Notes: (**A**) Schematic illustration of the structure of the NP, (**B**) SEM image of the NPs, (**C**) Size distribution of NPs by DLS measurement, (**D**) Zeta potential distribution of the NPs, (**E**) The detection of the folate on the surface of the NPs by laser scanning confocal microscopy.

Abbreviations: FA, folic acid; PEG, polyethylene glycol; PLGA, poly(lactide-*co*-glycolic acid); Ptx, paclitaxel; ICG, indocyanine green; Pfh, perfluorohexane; NPs, nanoparticles; FITC, fluorescein isothiocyanate; DiI, 1,1′-dioctadecyl-3,3,3′,3′-tetramethylindocarbocyanine perchlorate.

by dynamic light scattering and determined to be 308±5.82 nm (Figure 1C), which was consistent with the SEM findings. NP polydispersity index value was 0.087±0.041, indicating that their size was homogeneous. NP ζ-potential was −22.2±6.4 mV (Figure 1D). A negative surface charge can prolong NP blood circulation and prevent cytotoxicity caused by the proton-sponge effect.[26,27]

The binding ability of the folate on the surface of the NPs is crucial for targeting folate receptors, which is through ligand–receptor interaction. As such, we used immunofluorescence to discover whether this function was destroyed during fabrication. The NP shell was labeled by DiI, which appears red under CLSM. After incubation with the antibody against folate and the secondary antibody labeled with fluorescein isothiocyanate, FA-PEG-PLGA-Ptx@ICG-Pfh NPs appeared in green, which demonstrated the binding ability of folate was preserved (Figure 1E; PEG-PLGA-Ptx@ICG-Pfh NPs not shown). These results meant that FA-PEG-PLGA-Ptx@ICG-Pfh NPs had the potential to target the folate receptor.

NP photothermal effect and ability to change phase

ICG absorbed strongly in the NIR region: approximately 800 nm. With 808 nm NIR-laser irradiation, the temperature of the FA-PEG-PLGA-Ptx@ICG-Pfh NP solutions increased quickly during the first 120 seconds and tended to be stable after 160 seconds (Figure 2A). Meanwhile, the range and speed of the temperature increase were related to the concentration of the NPs. The temperature rapidly exceeded 42°C during the short irradiation period in the 6 mg/mL, 8 mg/mL, and 10 mg/mL groups, which is a crucial temperature point for triggering cancer-cell damage.[28] Compared with normal tissue, tumor tissue is much more vulnerable to heat because of the lower heat dissipation caused by poor vascularization,[29] indicating that due to their excellent photothermal conversion ability, these NPs have the potential for cancer PTT. Meanwhile, with increasing temperature, liquid Pfh can convert to a gaseous state. Therefore, to evaluate whether the NPs could be activated by laser irradiation, which is crucial for US imaging, a phase-change procedure was observed under microscopy. As shown in Figure 2B, no microbubbles were observed before irradiation. NPs began to expand after 50 seconds of irradiation. With continuous irradiation, many microbubbles were generated, especially after 200 seconds. This finding indicates that when converting to microbubbles, the NPs could be used as contrast agents for US imaging.

Drug loading and laser-triggered drug release

US-triggered drug release has been studied widely in the past few decades,[30] and due to the excellent photothermal conversion efficiency and phase-change ability of the FA-PEG-PLGA-Ptx@ICG-Pfh NPs and to discover whether the laser could trigger drug release, the drug-release behavior of the NPs was studied. First, the EE and LC of ICG and Ptx were detected (Table 1). The release behavior is shown in Figure 2C, and there were no significant differences in the cumulative release of Ptx between the two groups before laser irradiation (0.5 and 1 hour). After laser irradiation, a sharp increase in release was observed in FA-PEG-PLGA-Ptx@ICG-Pfh NPs with laser irradiation, while the cumulative release ratio increased slowly and constantly in FA-PEG-PLGA-Ptx@ICG-Pfh NPs without laser irradiation. These results indicate that the laser triggered sharp release of Ptx from the NPs, which may have provided a higher concentration of Ptx to the tumor region, leading to an improved therapeutic effect and fewer side effects.[31,32]

In vitro gel experiments of PA and US imaging

Multimodal imaging has been studied widely in recent years.[33] A specific imaging modality has its own advantages, but also some weaknesses. Multimodal imaging, such as US imaging combined with computed tomography, fluorescence imaging combined with magnetic resonance imaging, and nuclear imaging combined with magnetic resonance imaging have overcome these weaknesses to a certain extent.[34–36] PA imaging, a novel modality derived from PA effects, has the advantage of a high resolution because of its optical imaging character.[37] US is a safe and relatively inexpensive examination method that is used widely in clinical settings. In particular, CEUS can facilitate the detection and characterization of liver, breast, and thyroid focal lesions.[38–40] Therefore, we constructed FA-PEG-PLGA-Ptx@ICG-Pfh NPs as dual-modality contrast agents for PA and US imaging. In the in vitro gel experiment of PA imaging, spectra of the NPs within the NIR region were analyzed by the PA-imaging system. The PA signal peaked at 800 nm (Figure S2), due to the excellent absorption of ICG,[41] which was selected as the excitation NIR wavelength in the following experiments. As shown in Figure 2D and E, the PA signal strengthened linearly with increased concentration of FA-PEG-PLGA-Ptx@ICG-Pfh NPs from 2 to 10 mg/mL. In contrast, PBS alone produced a negligible PA signal, indicating that the NPs had the potential to serve as a PA contrast agent. In the in vitro gel experiment of US imaging, the signal was obtained before and during laser irradiation at different times. As shown in Figure 2F–H, before

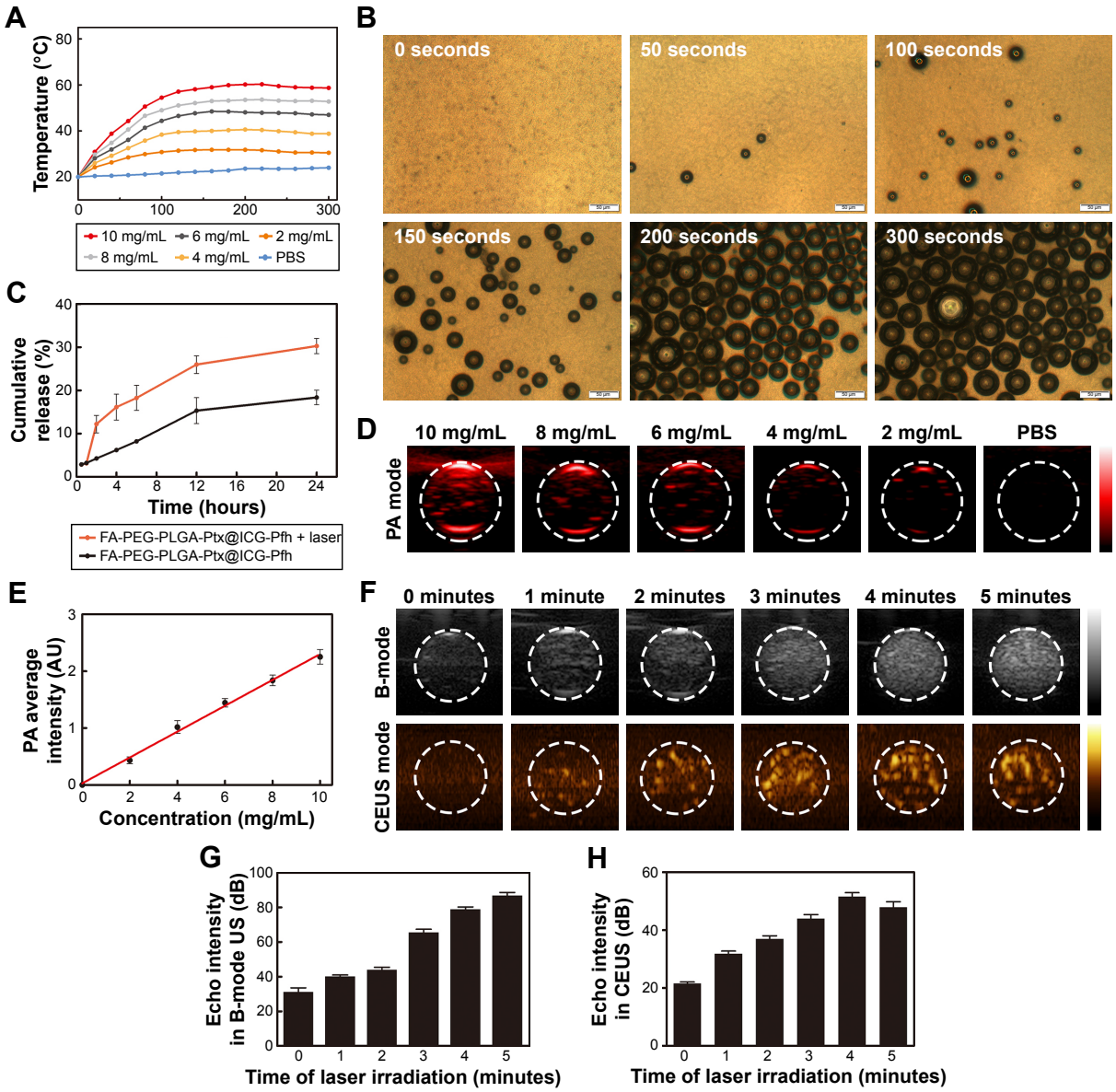

Figure 2 Photothermal effect, phase change, drug-release behavior, and in vitro PA and US imaging of FA-PEG-PLGA-Ptx@ICG-Pfh NPs.

Notes: (**A**) The concentration-dependent Photothermal heating curves of the NPs for 5 min laser irradiation. (**B**) Images of phase change of the NPs by microscopy. (**C**) Release behavior of Ptx from the FA-PEG-PLGA-Ptx@ICG-Pfh NPs with or without laser irradiation, (**D**) PA signals of the NPs at different concentrations, (**F**) B-mode and contrast enhanced ultrasound (CEUS) imaging of the NPs with the laser irradiation in phantom gel model, (**E**) Linearity curve of the PA signal and the concentration of NPs, (**G**) and (**H**) Echo intensity in B-mode and CEUS mode of NPs with the laser irradiation at different time.

Abbreviations: PA, photoacoustic; US, ultrasound; FA, folic acid; PEG, polyethylene glycol; PLGA, poly(lactide-*co*-glycolic acid); Ptx, paclitaxel; ICG, indocyanine green; Pfh, perfluorohexane; NPs, nanoparticles; CEUS, contrast-enhanced US.

laser irradiation, there was no US enhancement in B-mode or CEUS mode. When NPs were irradiated for 1 minute, minimal US enhancement was observed. Enhancement of both imaging modes peaked at 4 minutes. Unfortunately, the enhancement decreased slightly at 5 minutes (Figure 2H). It might be that large numbers of microbubbles were generated with continuous irradiation, and some of these microbubbles may have escaped from the transducer-detection layer by moving to the upper level via buoyancy, or some of these microbubbles were broken by the continuous expansion.

Table 1 Encapsulation EE and LC of ICG and Ptx

Reagent	EE (%)	LC (%)
ICG	27.15±3.27	0.97±0.11
Ptx	71.71±7.89	6.69±0.69

Abbreviations: ICG, indocyanine green; Ptx, paclitaxel; EE, encapsulation efficiency; LC, loading content.

Cytotoxicity and in vitro cellular uptake

The cytotoxicity of the FA-PEG-PLGA@ICG-Pfh NPs (Ptx-free) as a drug-delivery vehicle was evaluated by CCK8

assay using MDA-MB231 cells, A549 cells, and HUVECs (Figure 3A). No obvious cytotoxicity was observed after incubating the cells with different concentrations of FA-PEG-PLGA@ICG-Pfh NPs for 24 hours. There were no significant differences among any of the groups. Even when cells were incubated with the NPs at 8 mg/mL, the viability of the treated groups was >80%, indicating that the FA-PEG-PLGA@ICG-Pfh NPs made from safe and FDA-approved materials are biocompatible.

CLSM was used to evaluate the cellular uptake efficiency of the NPs, and fluorescence-labeling experiments (red fluorescence from DiI-labeled NPs and blue fluorescence from DAPI-labeled nuclei) were performed using four groups (group 1, FA-PEG-PLGA@ICG-Pfh NPs incubated with MDA-MB231 folate-receptor-overexpressing cells; group 2, PEG-PLGA@ICG-Pfh NPs incubated with MDA-MB231 cells; group 3, FA-PEG-PLGA@ICG-Pfh NPs incubated with A549 folate-receptor-underexpressing cells; and group 4, FA-PEG-PLGA@ICG-Pfh NPs incubated with MDA-MB231 cells with antagonized folate receptors). With continuous incubation, more red dots representing NPs were phagocytized by the cells in each group. After a 2-hour incubation, extensive red fluorescence was visible in the cytoplasm of MDA-MB231 cells in group 1, while less red fluorescence was observed in MDA-MB231 cells in group 2 than in group 1 and minimal red fluorescence observed in A549 cells in group 3. Furthermore, the red fluorescence signal was largely decreased in MDA-MB231 cells with antagonized folate receptors (Figure 3B). This could be because the folate-functionalized NPs bound much more easily to the folate-receptor-overexpressing MDA-MB231 cells through ligand–receptor interactions. As such, there were minimal folate-functionalized NPs in folate-receptor-underexpressing A549 cells. Conversely, as the folate receptors of the MDA-MB231 cells in group 4 were preoccupied, the number of folate-functionalized NPs decreased remarkably in these cells. These results show that the folate-ligand receptor could play a significant role in mediating MDA-MB231-cell phagocytosis of folate-functionalized NPs and indicate that FA-PEG-PLGA@ICG-Pfh NPs can target folate-overexpressing cancer cells, which might be utilized in targeted cancer therapy.

Anticancer effect

In light of the outstanding photothermal effect, sharp laser-triggered drug release and cancer-cell-targeting ability, the anticancer effect of the FA-PEG-PLGA-Ptx@ICG-Pfh NPs was evaluated in MDA-MB231 cells by CCK8 assay. As shown in Figure 3C, the viability of MDA-MB231 cells in FA-PEG-PLGA-Ptx@ICG-Pfh NPs with laser irradiation was lower than that of cells in FA-PEG-PLGA-Ptx@ICG-Pfh NPs without laser irradiation and FA-PEG-PLGA@ICG-Pfh (Ptx-free) NPs with laser irradiation. These results suggest that PTT combined with chemotherapy exerts a synergistic anticancer effect. Cell viability in FA-PEG-PLGA-Ptx@ICG-Pfh NPs with laser irradiation was lower than that in PEG-PLGA-Ptx@ICG-Pfh NPs with laser irradiation, indicating that targeted NPs improved anticancer efficacy. It could be that with folate-receptor mediation, more NPs were phagocytosed by MDA-MB231 cells, leading to enhanced PTT and

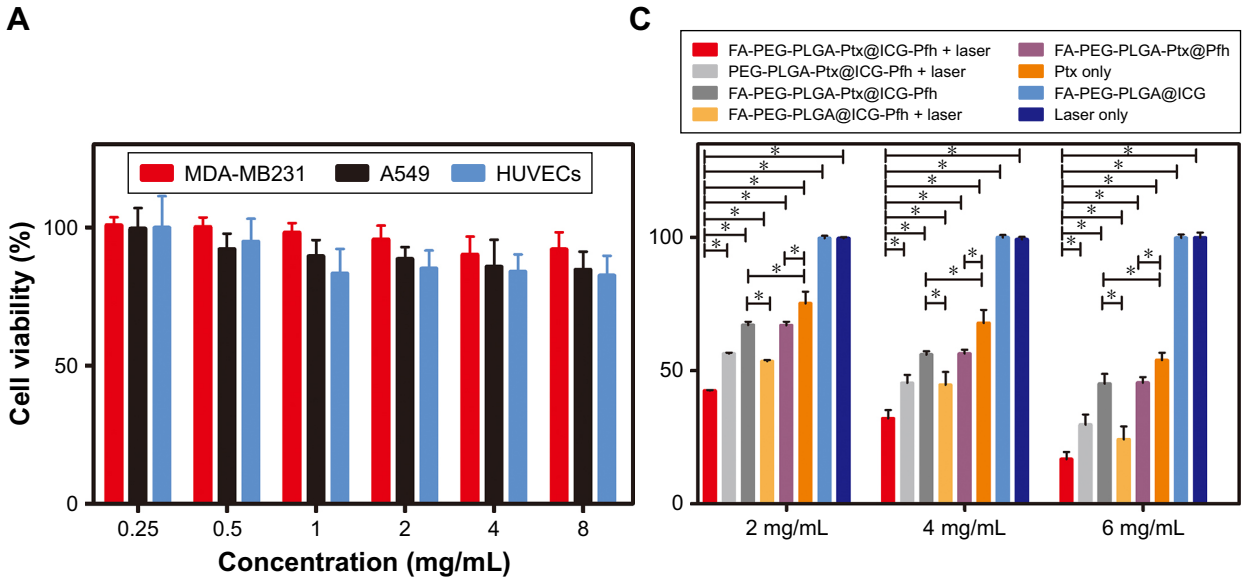

Figure 3 (*Continued*)

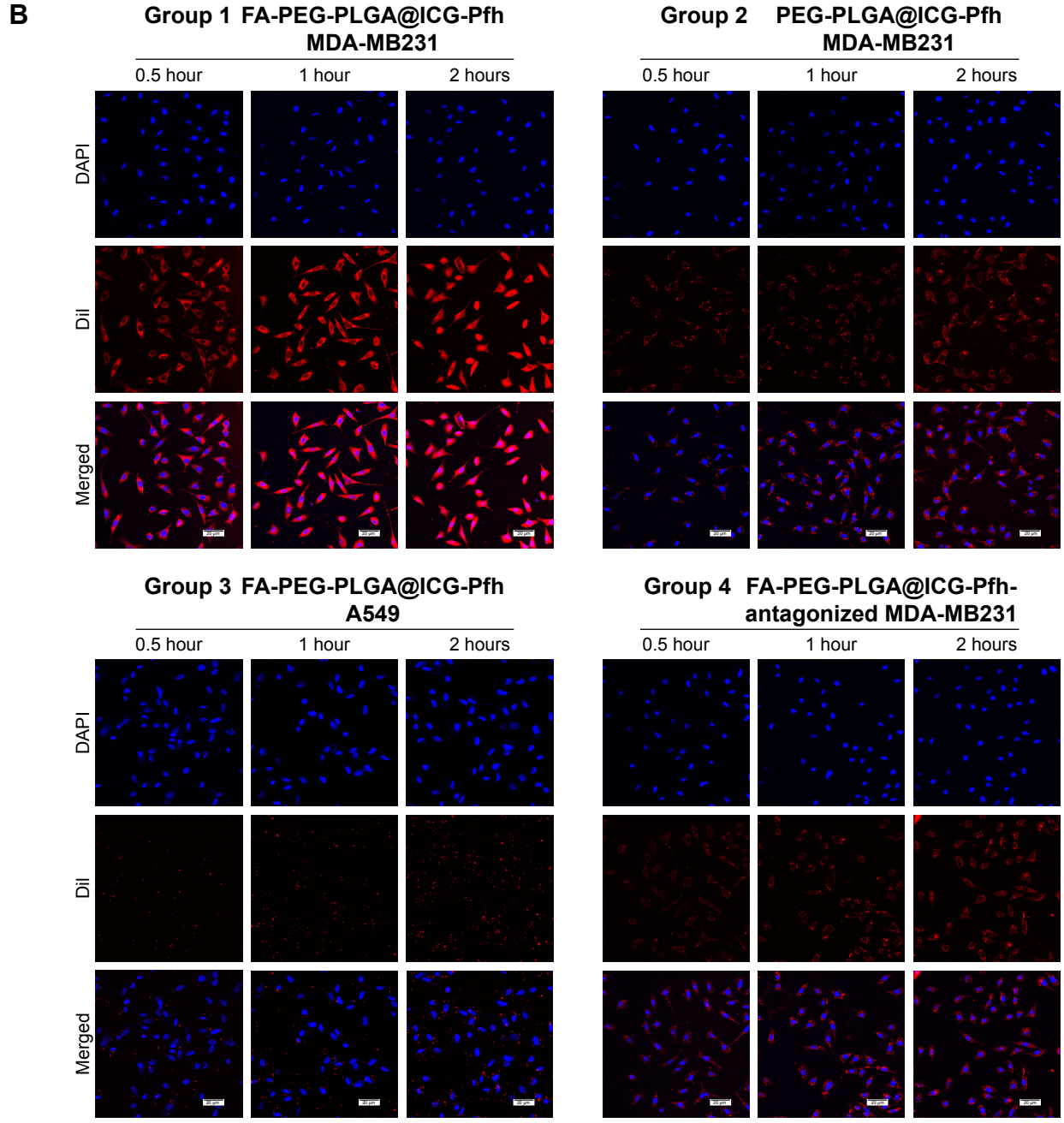

Figure 3 Cytotoxicity, in vitro cellular uptake, and anticancer effect of NPs.
Notes: (**A**) Cytotoxicity against MDA-MB231 cells, A549 cells, and HUVECs after incubation with FA-PEG-PLGA@ICG-Pfh NPs (Ptx-free) for 24 hours. (**B**) Cellular uptake of different groups; DAPI (blue) marks nuclei and DiI (red) PLGA NPs. (**C**) Anticancer efficacy of different therapies against MDA-MB231 cells. *$P<0.05$.
Abbreviations: NPs, nanoparticles; HUVECs, human umbilical vein endothelial cells; FA, folic acid; PEG, polyethylene glycol; PLGA, poly(lactide-*co*-glycolic acid); Ptx, paclitaxel; ICG, indocyanine green; Pfh, perfluorohexane.

chemotherapy efficacy. Furthermore, the cell viability of FA-PEG-PLGA@ICG-Pfh (Ptx-free) NPs with laser irradiation was lower than that of FA-PEG-PLGA-Ptx@ICG-Pfh NPs without laser irradiation. Even though FA-PEG-PLGA@ICG-Pfh NPs were not loaded with Ptx, cell viability was lower with these NPs under laser irradiation than that of NPs loaded with Ptx without laser irradiation. This finding indicates that PTT could play a leading role in the anticancer effect. Additionally, to a certain extent, this result could be ascribed to the direct destruction of the expanding bubbles, because the NPs within the cell were activated by laser irradiation and the cell directly destroyed by the expanding bubbles.[21] Additionally, compared with the Ptx-only group, the cell viability of FA-PEG-PLGA-Ptx@ICG-Pfh

NPs without laser irradiation was reduced. It may be that as a targeted drug-delivery vehicle, the folate-functionalized NPs loaded with Ptx passed through the cell membrane more easily than free Ptx, because folate or folate-modified NPs can be taken efficiently up by cells through receptor-mediated endocytosis.[42,43] NIR-radiation therapy has been studied widely and safely used in physical therapy to mitigate inflammation, alleviate edema, diminish pain, and accelerate bone healing after surgery.[44–47] Cialdai et al found that using an 808 nm NIR laser did not affect the behavior of breast adenocarcinoma cell lines in terms of proliferation, cell-cycle progression, apoptosis, or cloning efficiency.[48] Due to the excellent biosafety of the 808 nm NIR laser, there was barely any cytotoxicity in the laser-only group (Figure 3C). These results further indicate that PTT is a safe method for clinical application. Lastly, repeating this experiment using different concentrations of NPs yielded similar results, and efficacy improved with increasing concentrations.

In vivo biocompatibility

Animal experiments were carried out to study further the dual-modality imaging and therapeutic effect of the NPs in vivo. First, we detected the biocompatibility of NPs in vivo, which is crucial to future clinical translation. Traditional chemotherapy is an effective treatment for cancer, but it has some undesirable side effects.[49] Therefore, we evaluated routine blood indicators and detected some specific and representative indicators of liver and renal function. Compared with the control, there were no significant differences in liver function, renal function, or routine blood-test results in the groups administered NPs (Table 2). In particular, the number of white blood cells and platelets did not decrease, indicating that there was no significant marrow suppression. This excellent result could be ascribed to the safe and biocompatible materials and the targeted nature of the drug-delivery system, because the targeted drug carrier transported the chemotherapeutic agent to the tumor region, thereby avoiding normal tissue and reducing toxicity in the rest of the body.[50] In light of the excellent biocompatibility, a high dose of 50 mg/kg was selected for the following in vivo experiments.

Biodistribution and tumor accumulation of NPs

Based on to the remarkable ability of the folate-functionalized NPs to target folate-receptor-overexpressing tumor cells in vitro, biodistribution and tumor accumulation of the

Table 2 Liver function, renal function, and routine blood-test data of mice at day 7 after intravenous injection of FA-PEG-PLGA-Ptx@ICG-Pfh NPs at 10, 25, and 50 mg/kg

Dose of NP	Liver function				Renal function				Routine blood tests						
	ALT (U/L)	*P*-value	AST (U/L)	*P*-value	BUN (mg/dL)	*P*-value	Cr (μmol/L)	*P*-value	WBCs (10^9/L)	*P*-value	RBCs (10^{12}/L)	*P*-value	Hb (g/L)	*P*-value	Plt (10^9/L)	*P*-value
10 mg/kg	39.36±4.75	0.106	107.40±25.23	0.148	21.57±2.16	0.156	76.30±17.14	0.845	3.2±0.8	0.661	9.24±0.46	0.906	134±5	0.693	528±313	0.928
25 mg/kg	42.16±9.00	0.256	134.92±65.84	0.490	20.70±2.36	0.308	82.31±9.70	0.796	3.0±0.9	0.418	9.01±0.60	0.822	134±11	0.722	507±65	0.798
50 mg/kg	43.00±4.93	0.325	145.23±25.89	0.693	19.17±2.90	0.773	84.87±24.78	0.652	3.1±1.0	0.492	8.76±0.30	0.557	133±5	0.595	634±208	0.463
Saline	48.30±12.01		158.79±76.01		18.58±4.65		78.89±23.60		3.5±1.2		9.16±1.94		138±29		540±117	

Abbreviations: FA, folic acid; PEG, polyethylene glycol; PLGA, poly(lactide-*co*-glycolic acid); Ptx, paclitaxel; ICG, indocyanine green; Pfh, perfluorohexane; NPs, nanoparticles; BUN, blood urea nitrogen; Cr, creatinine; WBCs, white blood cells; RBCs, red blood cells; Hb, hemoglobin; Plt, platelet; ALT, alanine aminotransferase; AST, aspartate aminotransferase.

FA-PEG-PLGA-Ptx@ICG-Pfh NPs were studied in vivo. NPs labeled by DiR, an NIR probe, were intravenously injected (50 mg/kg) into tumor-bearing mice and fluorescence images taken at different points before and after administration. As shown in Figure 4A, fluorescent signals were hardly observed in the folate-functionalized NPs or non-folate-functionalized NPs before the injection. The fluorescent signal of the tumor region slightly increased at 0.5 hours postinjection in both groups, but there was no significant difference between the two groups. The fluorescent signal of the tumor region peaked at 1 hour postinjection in both groups, which provided an optimal therapeutic time window for subsequent anticancer therapy in vivo (Figure 4B). Obviously, the signal of the tumor region was higher in the FA-PEG-PLGA-Ptx@ICG-Pfh group than in the PEG-PLGA-Ptx@ICG-Pfh group from 1 hour postinjection to 24 hours postinjection. In particular, FA-PEG-PLGA-Ptx@ICG-Pfh NPs exhibited relatively longer retention in the tumor region. In addition, both groups exhibited extremely high fluorescent signals in the liver and spleen, owing to the rapid uptake of NPs by the reticuloendothelial system, which is abundant in the liver and spleen.[51] After in vivo imaging, mice were killed and tumor tissue and main organs excised for analysis. The signal was still visible in the tumor tissue of the FA-PEG-PLGA-Ptx@ICG-Pfh group. In contrast, there was hardly any signal in the tumor tissue of the PEG-PLGA-Ptx@ICG-Pfh group (Figure 4C and D). These results indicate that although the non-folate-functionalized NPs accumulated to tumor tissue effectively via the EPR effect,[52] folate-functionalized NPs leveraged not only the EPR effect but also ligand–receptor interactions for targeted binding, facilitating superior accumulation.

In vivo dual-modality PA–US imaging

In light of the excellent dual-modality PA–US imaging of folate-functionalized NPs in vitro, the ability of the NPs to facilitate PA and US imaging was studied in tumor-bearing mice. Compared with whole-body fluorescence imaging, PA imaging can image a region of interest, but with higher resolution and deeper imaging depth. It can be used to visualize microscopic biological tissue, such as solid-tumor tissue and inner vasculature.[53,54] As shown in Figure 4E and F, tissue and hemoglobin showed negligible absorption in the 800 nm excitation spectra, and a weak PA signal was observed before the injection. The PA signal in the tumor region increased slightly at 0.5 hours postinjection in both groups, but there was no significant difference between the two groups. The PA signal in the tumor region peaked at 1 hour postinjection in both groups, and the signal of the folate-functionalized NP group was approximately twice as strong than that of the non-folate-functionalized NP group. Additionally, the PA signal of the folate-functionalized NP group lasted longer than the non-folate-functionalized NP group. These results were consistent with the in vivo fluorescence-imaging results and confirmed that the FA-PEG-PLGA-Ptx@ICG-Pfh NPs accumulated effectively in tumor tissue. In addition, the optimal time for PTT is 1 hour after the injection, because of the maximum accumulation of FA-PEG-PLGA-Ptx@ICG-Pfh NPs in the tumor. As FA-PEG-PLGA-Ptx@ICG-Pfh NPs can be activated into microbubbles, NPs were studied in vivo as US-imaging agents. At 1 hour after intravenous injection, the tumor region was irradiated by NIR laser. As shown in Figure 4G–I, obvious enhancement was observed in CEUS mode after laser irradiation in the FA-PEG-PLGA-Ptx@ICG-Pfh group, while weak enhancement was observed in the PEG-PLGA-Ptx@ICG-Pfh group. This result could be ascribed to the excellent targeting ability of the folate-functionalized NPs and greater microbubble activation because of the higher temperature of the irradiated-tumor region in the FA-PEG-PLGA-Ptx@ICG-Pfh group, which is verified in the following section. Furthermore, although there was a significant difference between the folate-functionalized group and the non-folate-functionalized group after irradiation in B mode (Figure 4H), it was still very difficult to distinguish the difference by observation. Fortunately, in CEUS mode, the images were greatly improved, which is another reason why CEUS is used widely in the clinic.

In vivo anticancer therapy

Finally, the in vivo synergistic anticancer efficacy of FA-PEG-PLGA-Ptx@ICG-Pfh NPs by integrating PTT and targeted chemotherapy was evaluated. When the tumor volume grew to approximately 0.5 cm^3, MDA-MB231 breast cancer tumor-bearing mice were randomly divided into nine groups (n=8/group): FA-PEG-PLGA-Ptx@ICG-Pfh NPs with laser irradiation, PEG-PLGA-Ptx@ICG-Pfh NPs with laser irradiation, FA-PEG-PLGA-Ptx@ICG-Pfh NPs without laser irradiation, FA-PEG-PLGA@ICG-Pfh NPs with laser irradiation, FA-PEG-PLGA-Ptx@Pfh, Ptx only, FA-PEG-PLGA@ICG, laser only, and saline. At 1 hour after intravenous injection, the tumor regions of the corresponding groups were irradiated by NIR laser for 5 minutes at 2 W/cm^2 (808 nm). Meanwhile, the temperature of the tumor region was monitored by thermal imaging camera during irradiation. As shown in Figure 5A and B, the temperature increased slightly to 37.5°C in the laser-only group, which was lower than the 42°C hyperthermia threshold.[28] This finding indicates that the 808 nm NIR laser

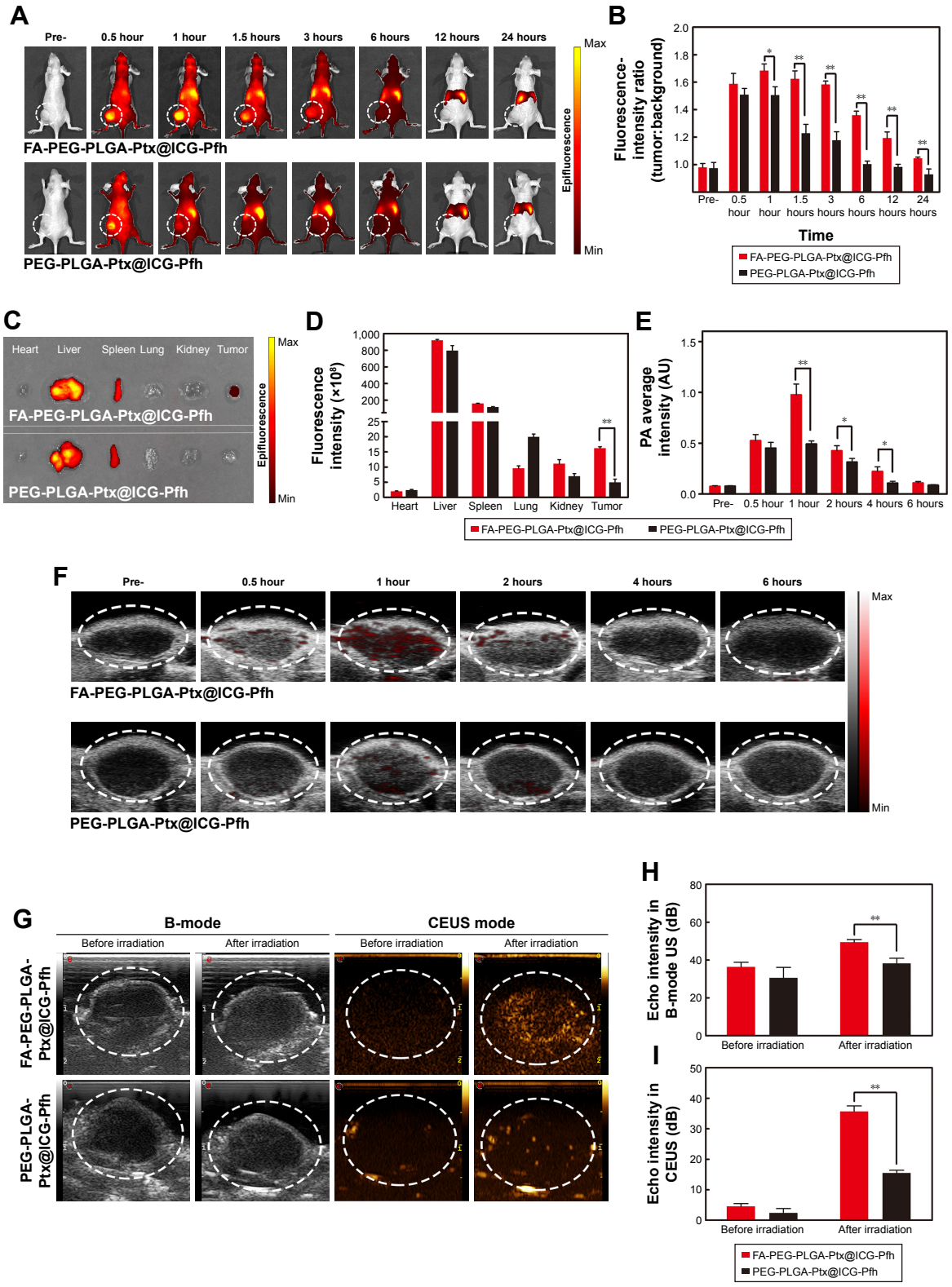

Figure 4 Biodistribution and tumor accumulation and in vivo PA and US imaging of FA-PEG-PLGA-Ptx@ICG-Pfh NPs.

Notes: (**A**) Biodistribution of NPs in MDA-MB231 tumor-bearing mice by in vivo fluorescent imaging; (**B**) fluorescence intensity (tumor:background) ratio of MDA-MB231 tumor-bearing mice administered NPs; (**C**) fluorescence imaging of main organs and tumors 24 hours after injection of FA-PEG-PLGA-Ptx@ICG-Pfh or PEG-PLGA-Ptx@ICG-Pfh NPs; (**D**) fluorescence intensity of main organs and tumors after 24 hours after of NPs; (**E**) average PA intensity of ROI after intravenous injection of NPs at different time points; (**F**) PA imaging of intravenously injected NP accumulation in MDA-MB231 tumor-bearing mice at different time points; (**G**) US monitoring of NIR laser irradiation 1 hour after intravenous injection of NPs in MDA-MB231 tumor-bearing mice; (**H**) echo intensity of ROI in B-mode US before and after laser irradiation; (**I**) echo intensity of ROI in CEUS before and after laser irradiation. *$P<0.05$; **$P<0.01$.

Abbreviations: PA, photoacoustic; US, ultrasound; FA, folic acid; PEG, polyethylene glycol; PLGA, poly(lactide-*co*-glycolic acid); Ptx, paclitaxel; ICG, indocyanine green; Pfh, perfluorohexane; NPs, nanoparticles; ROI, region of interest; CEUS, contrast-enhanced US.

is almost harmless to normal tissue and suitable for future clinical translation. While the temperature increased rapidly to 50.5°C and 50.6°C in FA-PEG-PLGA-Ptx@ICG-Pfh NPs with laser irradiation and FA-PEG-PLGA@ICG-Pfh NPs with laser irradiation, respectively, there was no significant difference between the two groups, indicating that regardless of whether folate-functionalized NPs were loaded with Ptx, PTT efficacy was not affected. Additionally, compared with the folate-functionalized groups, the temperature was lower in PEG-PLGA-Ptx@ICG-Pfh NPs with laser irradiation,

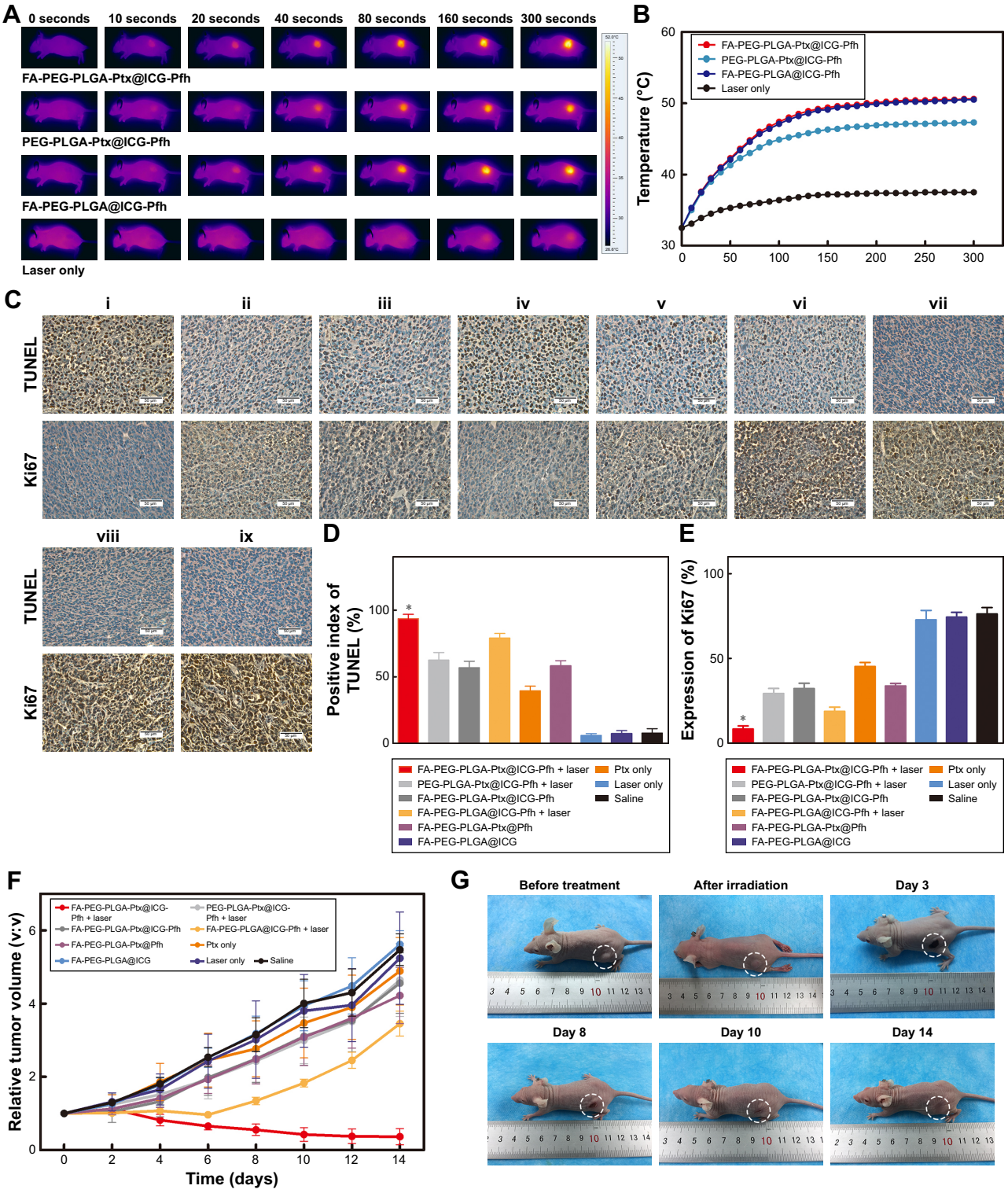

Figure 5 (*Continued*)

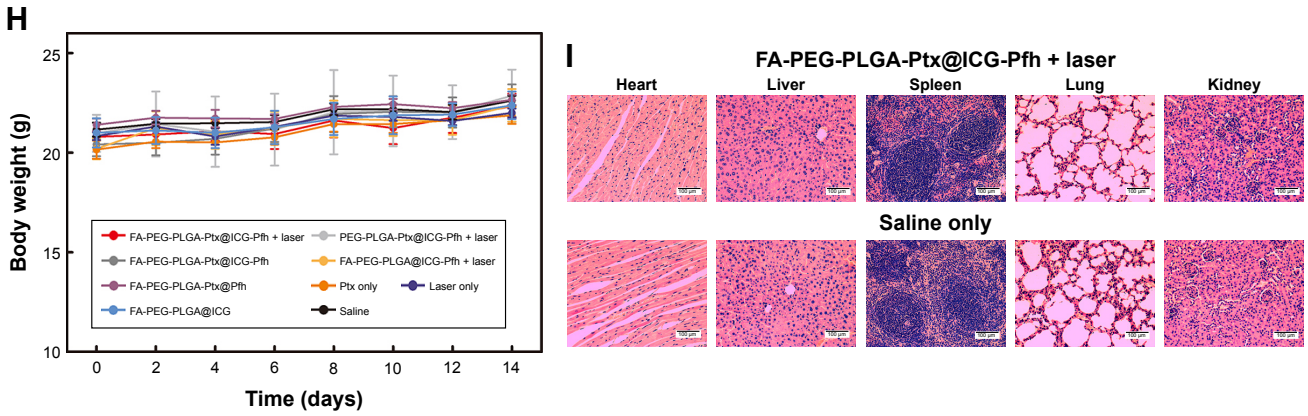

Figure 5 In vivo anticancer therapy.

Notes: (**A**) Monitoring images of MDA-MB231 tumor-bearing mice in laser-irradiation groups during PTT by thermal imaging. (**B**) Temperature of tumor region in laser-irradiation groups during PTT. (**C**) TUNEL and Ki67 expression in tumor tissue by immunohistochemical staining. Nuclei, stained in brown, are from TUNEL-positive or Ki67-positive cells, with blue indicating negative (FA-PEG-PLGA-Ptx@ICG-Pfh NPs with laser irradiation [i], PEG-PLGA-Ptx@ICG-Pfh NPs with laser irradiation [ii], FA-PEG-PLGA-Ptx@ICG-Pfh NPs without laser irradiation [iii], FA-PEG-PLGA@ICG-Pfh NPs with laser irradiation [iv], FA-PEG-PLGA-Ptx@Pfh without laser irradiation [v], Ptx only [vi], FA-PEG-PLGA@ICG without laser irradiation [vii], laser only [viii], saline [ix]). (**D**) Positive index of TUNEL assay for FA-PEG-PLGA-Ptx@ICG-Pfh NPs with laser irradiation was higher than that in the other eight groups ($P<0.05$). (**E**) Ki67 expression for FA-PEG-PLGA-Ptx@ICG-Pfh NPs with laser irradiation was lower than that of the other eight groups ($P<0.05$). (**F**) Relative tumor-volume curves of different groups of MDA-MB231 tumor-bearing mice. (**G**) Typical MDA-MB231 tumor-bearing mice having received FA-PEG-PLGA-Ptx@ICG-Pfh with laser irradiation on different days. (**H**) Body weight of mice was measured during the 14 observation days in different groups. (**I**) H&E-staining images of major organs collected from the FA-PEG-PLGA-Ptx@ICG-Pfh NPs with laser irradiation and saline only (control) groups. *$P<0.05$ significant difference FA-PEG-PLGA-Ptx@ICG-Pfh compared with other groups.

Abbreviations: PTT, photothermal therapy; FA, folic acid; PEG, polyethylene glycol; PLGA, poly(lactide-*co*-glycolic acid); Ptx, paclitaxel; ICG, indocyanine green; Pfh, perfluorohexane; NPs, nanoparticles.

although the temperature exceeded the hyperthermia threshold. This finding suggests that due to the excellent targeting ability of the folate-functionalized NPs, more ICG encapsulated in the NPs accumulated in the tumor region, leading to higher temperatures. On the third day after treatment, three mice were randomly selected from each group and killed for immunohistochemical staining (Figure 5C). Ki67 expression and results of TUNEL assays have been recognized widely as indices of tumor proliferation and apoptosis, respectively.[55,56] As shown in Figure 5D, the positive index (PI) of the TUNEL assay in FA-PEG-PLGA-Ptx@ICG NPs with laser irradiation was higher than that in the other eight groups, indicating that the targeted chemo/phototherapy efficiently induce tumor-cell apoptosis. The PI of the TUNEL was greater in FA-PEG-PLGA@ICG-Pfh NPs (Ptx-free) with laser irradiation than in FA-PEG-PLGA-Ptx@ICG-Pfh NPs without laser irradiation group, indicating that PTT may play a leading role in combined anticancer therapy. Ki67 expression of was lowest in FA-PEG-PLGA-Ptx@ICG-Pfh NPs with laser irradiation among the groups, indicating that the targeted chemo/phototherapy significantly inhibited tumor-cell proliferation (Figure 5E). In addition, there were no significant differences in TUNEL PI or Ki67 expression between the laser-only and saline groups, indicating that the 808 nm NIR laser was safe for tissue at the molecular level. To evaluate synergistic anticancer efficacy further, tumor volumes was measured every 2 days and normalized against their original volume (day 0, Figure 5F). The saline (control) and laser-only groups each showed a fivefold increase in average tumor volume compared with original volume, and there was no significant difference between the two groups, indicating that MDA-MB231 tumor growth was not affected by 808 nm NIR-laser irradiation alone. Compared with the control group, tumor volume was inhibited slightly in the FA-PEG-PLGA-Ptx@ICG-Pfh NP and Ptx-only groups, and relative tumor volume was slightly smaller in FA-PEG-PLGA-Ptx@ICG-Pfh NPs, indicating that the targeted drug-delivery treatment was much more efficient than traditional chemotherapy. Obviously, compared with PEG-PLGA-Ptx@ICG-Pfh NPs with laser irradiation, tumor growth was significantly inhibited in FA-PLGA-PEG-Ptx@ICG-Pfh NPs with laser irradiation, and average tumor volume decreased by 63% compared with original volume, indicating that the targeted delivery system provided improved PTT and chemotherapy. Surprisingly, as shown in Figure 5G, the mice receiving FA-PLGA-PEG-Ptx@ICG-Pfh NPs with laser irradiation showed the best anticancer efficacy. Before treatment, tumors were evident in left hind limbs of mice. On day 3 after treatment, the tumor region began to scab. On day 8 after treatment, the wound began to heal. On day 10 after treatment, there was only a small scab surrounded by some scar tissue. On day 14 after treatment, the skin had almost recovered, and the tumor did not recur. Meanwhile, compared with FA-PEG-PLGA-Ptx@ICG-Pfh NPs, tumor

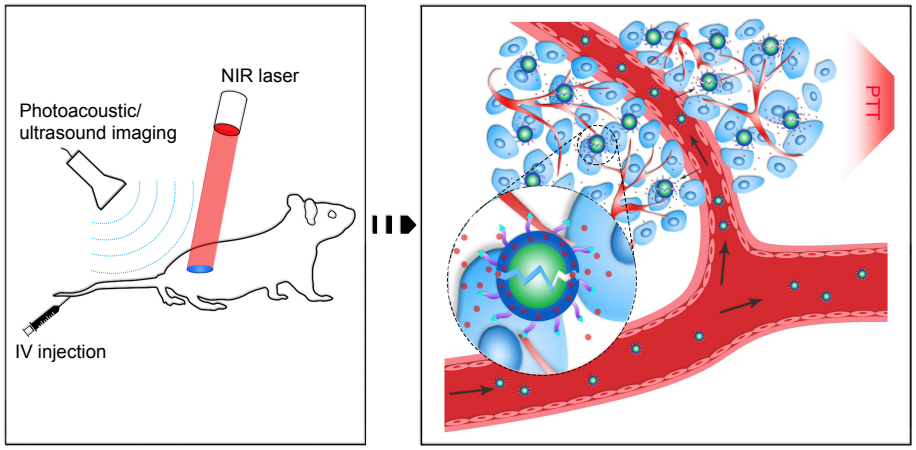

Figure 6 Schematic of the theranostic FA-PEG-PLGA-Ptx@ICG-Pfh NPs.
Abbreviations: FA, folic acid; PEG, polyethylene glycol; PLGA, poly(lactide-*co*-glycolic acid); Ptx, paclitaxel; ICG, indocyanine green; Pfh, perfluorohexane; NPs, nanoparticles; NIR, near-infrared; IV, intravenous; PTT, photothermal therapy.

volume was significantly decreased in FA-PEG-PLGA@ICG-Pfh NPs (Ptx-free) with laser irradiation, indicating that PTT could play a leading role in the anticancer effect of the synergistic therapy. Additionally, although the anticancer efficacy of FA-PEG-PLGA@ICG-Pfh NPs (Ptx-free) with laser irradiation was as good as that of FA-PEG-PLGA-Ptx@ICG-Pfh NPs with laser irradiation in the beginning, the tumor recurred 6 days later, indicating that targeted chemotherapy was necessary. Although PTT could play a leading role in the anticancer effect, targeted chemotherapy may serve a vital supplementary function. In summary, the folate-functionalized targeted drug-delivery system with combined PTT and chemotherapy achieved excellent synergistic anticancer efficacy that inhibited tumor recurrence.

Biotoxicity evaluation of chemo/photothermal therapy

In light of the excellent biocompatibility of the folate-functionalized NPs in vitro and in vivo, the biotoxicity of the chemo/photothermal synergistic therapy was evaluated. The body weight of the mice was monitored in all groups for 14 days. As shown in Figure 5H, compared with the saline group (control), there were no significant differences in the other treated groups, suggesting that the chemo/photothermal synergistic therapeutic procedure did not induce obvious side effects. Moreover, mice that were randomly selected from the FA-PEG-PLGA-Ptx@ICG-Pfh NPs with laser-irradiation and saline groups were killed at day 14 (n=3/group), and the main organs (heart, liver, spleen, lungs, and kidneys) excised for H&E staining. Compared with the saline group, no obvious changes in histomorphology or an abnormal inflammatory response of the main organs were observed in the FA-PEG-PLGA-Ptx@ICG-Pfh NPs-with-laser-irradiation group (Figure 5I), indicating that the chemo/photothermal synergistic therapy based on FA-PEG-PLGA-Ptx@ICG-Pfh NPs was safe and had low toxicity, which would make it possible for future clinical translation.

Conclusion

In this study, using safe and approved materials and drugs, we successfully constructed FA-PEG-PLGA-Ptx@ICG-Pfh NPs, folate receptor-targeted laser-activable PLGA NPs loaded with Ptx and ICG. This new class of biocompatible theranostic agents can be used in multiple capacities, including as a dual-modality agent for PA and US imaging and as a therapeutic agent that delivers Ptx and ICG to targeted regions to achieve excellent chemo/photothermal therapy. Moreover, with the targeted delivery system and phase-change ability, folate-functionalized NPs can be triggered by laser irradiation at the tumor region to induce sharp release of Ptx, leading to improved therapeutic efficacy and fewer side effects (Figure 6). Such a novel and biocompatible theranostic NP is expected to integrate dual-modality imaging with improved therapeutic efficacy and provide a promising paradigm for cancer therapy.

Acknowledgments

The authors are grateful to Dr Nan Zhang and Ju Huang for their assistance. This work was supported by the National Natural Science Foundation of China (grants 81501484, 81630047, 81471713, 31630026, and 81701709) and the University Innovation Team Plans of Chongqing, China (grant CXTDG201602007).

Disclosure

The authors report no conflicts of interest in this work.

References

1. Palekar-Shanbhag P, Jog SV, Chogale MM, Gaikwad SS. Theranostics for cancer therapy. *Curr Drug Deliv*. 2013;10(3):357–362.
2. Sankar PL, Parker LS. The Precision Medicine Initiative's All of Us Research Program: an agenda for research on its ethical, legal, and social issues. 2017;19(7):743–750.
3. Santurro A, Vullo AM, Borro M, et al. Personalized medicine applied to forensic sciences: new advances and perspectives for a tailored forensic approach. *Curr Pharm Biotechnol*. 2017;18(3):263–273.
4. D'Souza LS, Payette MJ. Estimated cost efficacy of systemic treatments that are approved by the US Food and Drug Administration for the treatment of moderate to severe psoriasis. *J Am Acad Dermatol*. 2015; 72(4):589–598.
5. Mailankody S, Prasad V. Five years of cancer drug approvals: innovation, efficacy, and costs. *JAMA Oncol*. 2015;1(4):539–540.
6. He H, Markoutsa E, Zhan Y, Zhang J, Xu P. Mussel-inspired PLGA/polydopamine core-shell nanoparticle for light induced cancer thermochemotherapy. *Acta Biomater*. 2017;59:181–191.
7. Chen Y, Jiang L, Wang R, et al. Injectable smart phase-transformation implants for highly efficient in vivo magnetic-hyperthermia regression of tumors. *Adv Mater*. 2014;26(44):7468–7473.
8. Saxena V, Sadoqi M, Shao J. Indocyanine green-loaded biodegradable nanoparticles: preparation, physicochemical characterization and in vitro release. *Int J Pharm*. 2004;278(2):293–301.
9. Sadat Tabatabaei Mirakabad F, Nejati-Koshki K, Akbarzadeh A, et al. PLGA-based nanoparticles as cancer drug delivery systems. *Asian Pac J Cancer Prev*. 2014;15(2):517–535.
10. Li B, Zhang XY, Yang JZ, et al. Influence of polyethylene glycol coating on biodistribution and toxicity of nanoscale graphene oxide in mice after intravenous injection. *Int J Nanomedicine*. 2014;9:4697–4707.
11. Pasut G, Panisello A, Folch-Puy E, et al. Polyethylene glycols: An effective strategy for limiting liver ischemia reperfusion injury. *World J Gastroenterol*. 2016;22(28):6501–6508.
12. Ma Y, Tong S, Bao G, Gao C, Dai Z. Indocyanine green loaded SPIO nanoparticles with phospholipid-PEG coating for dual-modal imaging and photothermal therapy. *Biomaterials*. 2013;34(31):7706–7714.
13. Kuo WS, Chang YT, Cho KC, et al. Gold nanomaterials conjugated with indocyanine green for dual-modality photodynamic and photothermal therapy. *Biomaterials*. 2012;33(11):3270–3278.
14. Hu D, Liu C, Song L, et al. Indocyanine green-loaded polydopamine-iron ions coordination nanoparticles for photoacoustic/magnetic resonance dual-modal imaging-guided cancer photothermal therapy. *Nanoscale*. 2016;8(39):17150–17158.
15. Matsuzaki M, Haruna M, Ota E, Sasaki S, Nagai Y, Murashima S. Dietary folate intake, use of folate supplements, lifestyle factors, and serum folate levels among pregnant women in Tokyo, Japan. *J Obstet Gynaecol Res*. 2008;34(6):971–979.
16. Chen C, Ke J, Zhou XE, et al. Structural basis for molecular recognition of folic acid by folate receptors. *Nature*. 2013;500(7463):486–489.
17. Assaraf YG, Leamon CP, Reddy JA. The folate receptor as a rational therapeutic target for personalized cancer treatment. *Drug Resist Updat*. 2014;17(4–6):89–95.
18. Mousnier L, Huang N, Morvan E, Fattal E, Tsapis N. Influence of polymer end-chemistry on the morphology of perfluorohexane polymeric microcapsules intended as ultrasound contrast agents. *Int J Pharm*. 2014; 471(1–2):10–17.
19. Zhou Y, Wang Z, Chen Y, et al. Microbubbles from gas-generating perfluorohexane nanoemulsions for targeted temperature-sensitive ultrasonography and synergistic HIFU ablation of tumors. *Adv Mater*. 2013;25(30):4123–4130.
20. Su YL, Fang JH, Liao CY, et al. Targeted mesoporous iron oxide nanoparticles-encapsulated perfluorohexane and a hydrophobic drug for deep tumor penetration and therapy. *Theranostics*. 2015;5(11): 1233–1248.
21. Sun Y, Wang Y, Niu C, et al. Laser-activatible PLGA microparticles for image-guided cancer therapy in vivo. *Adv Funct Mater*. 2014;24(48): 7674–7680.
22. Yang P, Li D, Jin S, et al. Stimuli-responsive biodegradable poly (methacrylic acid) based nanocapsules for ultrasound traced and triggered drug delivery system. *Biomaterials*. 2014;35(6):2079–2088.
23. Guo L, Yan DD, Yang D, et al. Combinatorial photothermal and immuno cancer therapy using chitosan-coated hollow copper sulfide nanoparticles. *ACS Nano*. 2014;8(6):5670–5681.
24. Nguyen HT, Phung CD, Thapa RK, et al. Multifunctional nanoparticles as somatostatin receptor-targeting delivery system of polyaniline and methotrexate for combined chemo-photothermal therapy. *Acta Biomater*. 2018;68:154–167.
25. Hu H, Xiao C, Wu H, et al. Nanocolloidosomes with selective drug release for active tumor-targeted imaging-guided photothermal/chemo combination therapy. *ACS Appl Mater Interfaces*. 2017;9(48): 42225–42238.
26. Chen J, Ding J, Wang Y, et al. Sequentially responsive shell-stacked nanoparticles for deep penetration into solid tumors. *Adv Mater*. 2017; 29(32):1701170.
27. Nel AE, Mädler L, Velegol D, et al. Understanding biophysicochemical interactions at the nano-bio interface. *Nat Mater*. 2009;8(7): 543–557.
28. Cherukuri P, Glazer ES, Curley SA. Targeted hyperthermia using metal nanoparticles. *Adv Drug Deliv Rev*. 2010;62(3):339–345.
29. Redolfi Riva E, Desii A, Sinibaldi E, et al. Gold nanoshell/polysaccharide nanofilm for controlled laser-assisted tissue thermal ablation. *ACS Nano*. 2014;8(6):5552–5563.
30. Jain A, Tiwari A, Verma A, Jain SK. Ultrasound-based triggered drug delivery to tumors. *Drug Deliv Transl Res*. 2018;8(1):150–164.
31. Di J, Kim J, Hu Q, Jiang X, Gu Z. Spatiotemporal drug delivery using laser-generated-focused ultrasound system. *J Control Release*. 2015; 220(Pt B):592–599.
32. He H, Markoutsa E, Zhan Y, Zhang J, Xu P. Mussel-inspired PLGA/polydopamine core-shell nanoparticle for light induced cancer thermochemotherapy. *Acta Biomater*. 2017;59:181–191.
33. Burke BP, Cawthorne C, Archibald SJ. Multimodal nanoparticle imaging agents: design and applications. *Philos Trans A Math Phys Eng Sci*. 2017;375(2107):20170261.
34. Zhang N, Li J, Hou R, et al. Bubble-generating nano-lipid carriers for ultrasound/CT imaging-guided efficient tumor therapy. *Int J Pharm*. 2017;534(1–2):251–262.
35. Lee JH, Kim JW, Cheon J. Magnetic nanoparticles for multi-imaging and drug delivery. *Mol Cells*. 2013;35(4):274–284.
36. Lamb JR, Holland JP. Advanced methods for radiolabelling nanomedicines for multi-modality nuclear/MR imaging. *J Nucl Med*. 2018;59(3):382–389.
37. Wang S, Lin J, Wang T, Chen X, Huang P. Recent Advances in Photoacoustic Imaging for Deep-Tissue Biomedical Applications. *Theranostics*. 2016;6(13):2394–2413.
38. Durot I, Wilson SR, Willmann JK. Contrast-enhanced ultrasound of malignant liver lesions. *Abdom Radiol*. 2017;1:1–29.
39. Xiang LH, Yao MH, Xu G, et al. Diagnostic value of contrast-enhanced ultrasound and shear-wave elastography forbreast lesions of subcentimeter. *Clin Hemorheol Microcirc*. 2017;67(1):69–80.
40. Schleder S, Janke M, Agha A, et al. Preoperative differentiation of thyroid adenomas and thyroid carcinomas using high resolution contrast-enhanced ultrasound (CEUS). *Clin Hemorheol Microcirc*. 2015;61(1):13–22.
41. Beztsinna N, Tsvetkova Y, Jose J, et al. Photoacoustic imaging of tumor targeting with riboflavin-functionalized theranostic nanocarriers. *Int J Nanomedicine*. 2017;12:3813–3825.
42. Zheng C, Zheng M, Gong P, et al. Indocyanine green-loaded biodegradable tumor targeting nanoprobes for invitro and invivo imaging. *Biomaterials*. 2012;33(22):5603–5609.
43. Yang J, Vlashi E, Low P. Folate-linked drugs for the treatment of cancer and inflammatory diseases. *Subcell Biochem*. 2012;56:163–179.
44. Albertini R, Villaverde AB, Aimbire F, et al. Anti-inflammatory effects of low-level laser therapy (LLLT) with two different red wavelengths (660 nm and 684 nm) in carrageenan-induced rat paw edema. *J Photochem Photobiol B*. 2007;89(1):50–55.

45. Radwan DA, Mohammed NH, Zaky AA. Effectiveness of low power laser therapy and betamethasone in minimizing postoperative edema and trismus after third molar surgery: a clinical trial. *J Am Sci*. 2010;6(12):986–989.
46. Abreu ME, Viegas VN, Pagnoncelli RM, et al. Infrared laser therapy after surgically assisted rapid palatal expansion to diminish pain and accelerate bone healing. *World J Orthod*. 2010;11(3):273–277.
47. de Morais NC, Barbosa AM, Vale ML, et al. Anti-inflammatory effect of low-level laser and light-emitting diode in zymosan-induced arthritis. *Photomed Laser Surg*. 2010;28(2):227–232.
48. Cialdai F, Landini I, Capaccioli S, et al. In vitro study on the safety of near infrared laser therapy in its potential application as postmastectomy lymphedema treatment. *Journal of photochemistry and photobiology. B, Biology*. 2015;151:285–296.
49. Iwamoto T. Clinical application of drug delivery systems in cancer chemotherapy: review of the efficacy and side effects of approved drugs. *Biol Pharm Bull*. 2013;36(5):715–718.
50. Pérez-Herrero E, Fernández-Medarde A. Advanced targeted therapies in cancer: drug nanocarriers, the future of chemotherapy. *Eur J Pharm Biopharm*. 2015;93:52–79.
51. Tartaro K, Vanvolkenburg M, Wilkie D, et al. Development of a fluorescence-based in vivo phagocytosis assay to measure mononuclear phagocyte system function in the rat. *J Immunotoxicol*. 2015;12(3):239–246.
52. Björnmalm M, Thurecht KJ, Michael M, Scott AM, Caruso F. Bridging bio-nano science and cancer nanomedicine. *ACS Nano*. 2017;11(10):9594–9613.
53. Guo M, Mao H, Li Y, et al. Dual imaging-guided photothermal/photodynamic therapy using micelles. *Biomaterials*. 2014;35(16):4656–4666.
54. Gao S, Wang G, Qin Z, et al. Oxygen-generating hybrid nanoparticles to enhance fluorescent/photoacoustic/ultrasound imaging guided tumor photodynamic therapy. *Biomaterials*. 2017;112:324–335.
55. Denkert C, Budczies J, von Minckwitz G, Wienert S, Loibl S, Klauschen F. Strategies for developing Ki67 as a useful biomarker in breast cancer. *Breast*. 2015;24(Suppl 2):S67–S72.
56. Mohan C, Long K, Mutneja M, Ma J. Detection of end-stage apoptosis by ApopTag(R) TUNEL technique. *Methods Mol Biol*. 2015;1219:43–56.

Supplementary materials

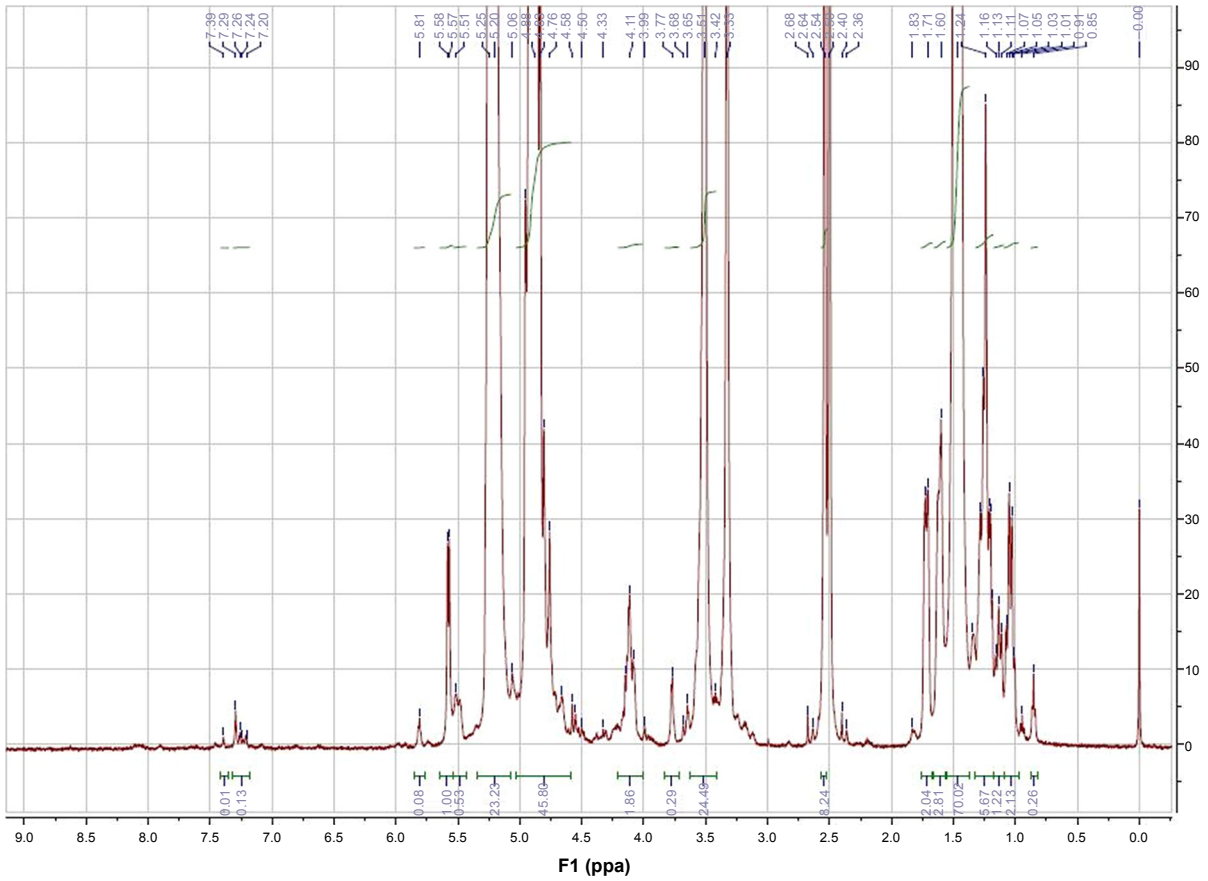

Figure S1 ^{1}H NMR spectra of the FA-PEG-PLGA polymer.
Abbreviations: NMR, nuclear magnetic resonance; FA, folic acid; PEG, polyethylene glycol; PLGA, poly(lactide-*co*-glycolic acid).

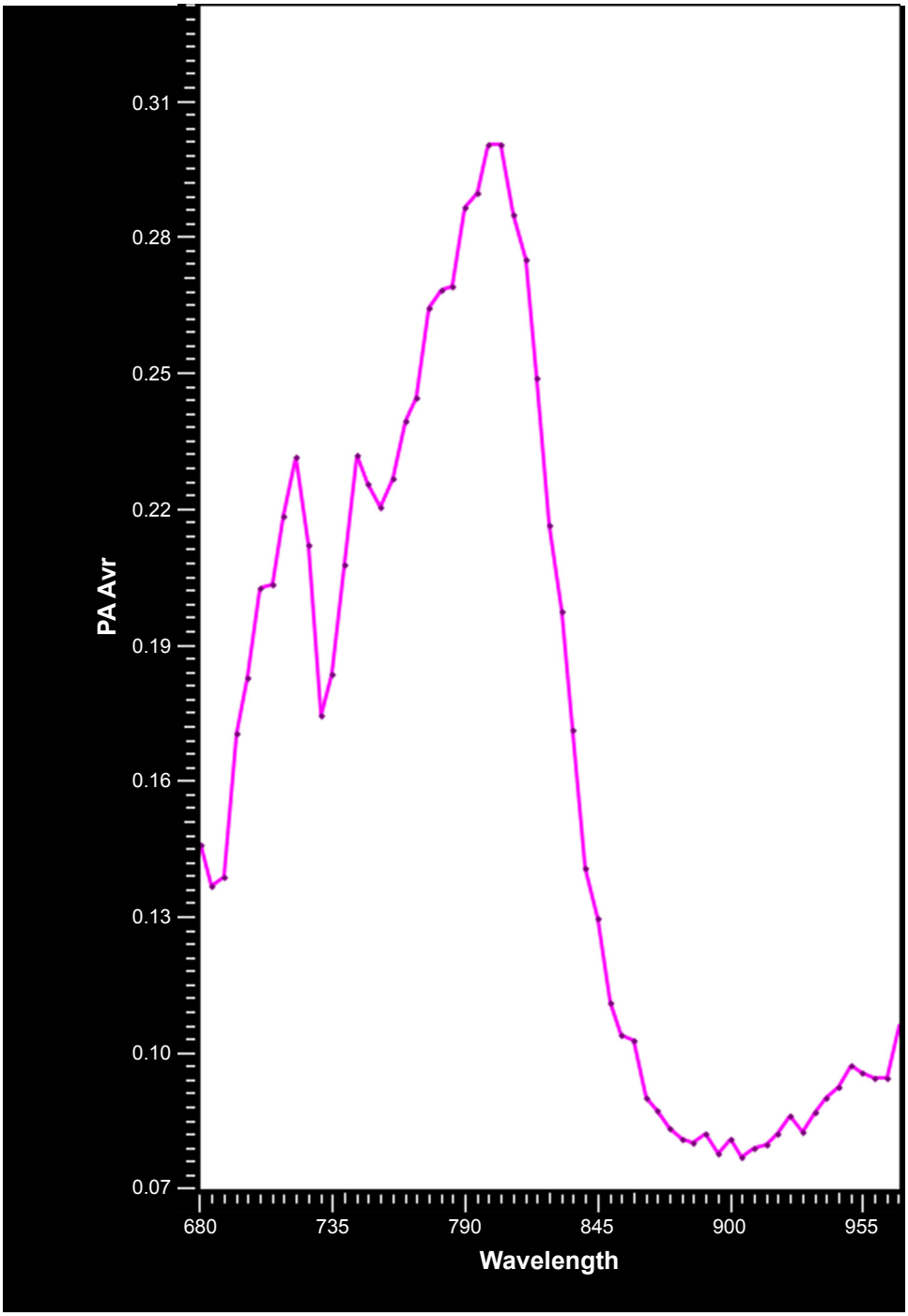

Figure S2 PA absorption spectrum of FA-PEG-PLGA-Ptx@ICG-Pfh NPs within excitation of NIR region (wavelength 680–970 nm).
Abbreviations: PA, photoacoustic; FA, folic acid; PEG, polyethylene glycol; PLGA, poly(lactide-*co*-glycolic acid); Ptx, paclitaxel; ICG, indocyanine green; Pfh, perfluorohexane; NPs, nanoparticles; NIR, near-infrared; Avr, verage intensity.